

Improved initial data for black hole collisions

Carlos O. Lousto* and Richard H. Price

Department of Physics, University of Utah, Salt Lake City, UT 84112

Numerical relativity codes now being developed will evolve initial data representing colliding black holes at a relatively late stage in the collision. The choice of initial data used for code development has been made on the basis of mathematical definitiveness and usefulness for computational implementation. By using the “particle limit” (the limit of an extreme ratio of masses of colliding holes) we recently showed that the standard choice is not a good representation of astrophysically generated initial data. Here we show that, for the particle limit, there is a very simple alternative choice that appears to give excellent results. That choice, “convective” initial data is, roughly speaking, equivalent to the start of a time sequence of parameterized solutions of the Hamiltonian constraint; for a particle in circular orbit, it is the initial data of the steady state solution on any hypersurface. The implementation of related schemes for equal mass holes is discussed.

I. INTRODUCTION

Recently the numerical computation of gravitational waves from coalescing black holes has received considerable attention and effort for closely related reasons. (i) The problem is a testbed for numerical relativity and has been the center of a collaboration of eight universities [1]. (ii) The results are necessary to understand details, and perhaps even gross features of coalescing black holes, presently viewed by many as the most promising source of gravitational waves detectable by earth based instruments [2,3]. (iii) The problem is interesting in its own regard as the first solution of Einstein’s equations for strong field interactions without simplifying symmetry.

The job of the numerical codes under development will be to evolve forward in time from an initial value solution on a starting hypersurface. There are many ways that initial data can be chosen to represent the starting state of two black holes. If the black holes are far apart on the initial hypersurface, then any reasonable choice of hypersurface data will suffice. Unfortunately the instabilities in evolution codes mean that the codes can only run for a relatively short time, and initial data will have to be specified on a hypersurface as late as possible.

For the most part, the initial data used to the present has been that put forth by York and Bowen, and coworkers [4–6]. This scheme starts by requiring that the initial geometry be conformally flat and that the extrinsic curvature have a property called “longitudinal,” equivalent to the condition that it be derivable from a vector potential. The solution is then made inversion symmetric, so that topological throats representing the black holes connect two isometric asymptotically flat universes. (This step of making the hypersurface data inversion symmetric turns out to destroy “longitudinality” [7].)

The advantages of this approach to initial data include the following: (i) Since it is widely adopted in the numerical relativity community, comparison of results of different groups is facilitated. (ii) It is specific and definitive and the numerical methods of solving for these initial data are highly developed [8]. (iii) The inversion symmetry gave a simple inner boundary condition for evolution codes. (iv) An argument could be made that the initial data was free of, or had a minimal content of, radiation encoded (in some sense) in the initial data themselves, so that the outgoing radiation found in a spacetime evolution should represent only the radiation due to the dynamical interaction of the black holes.

The Bowen-York (hereafter BY) scheme served very well in the role intended for it. One should ask, however, whether it is the appropriate scheme for computations supporting the search for gravitational waves. There are strong reasons for concluding that the answer is “no.” One immediate reason is that the Kerr geometry itself cannot be put in this scheme; a constant time slice of the Kerr geometry is not conformally flat. Even a single spinning BY hole will therefore radiate gravitational waves as it settles down into its Kerr final state [9].

A second rather direct reason comes from recent calculations we carried out for radiation from a particle falling radially into a Schwarzschild hole [10,11], hereafter Paper I and Paper II. In these calculations, the “particle” was taken as a perturbation of the background black hole spacetime and computations could be done relatively easily

*Electronic Address: lousto@mail.physics.utah.edu

for a variety of choices of data on an initial hypersurface. Furthermore, evolved data could be extracted on later hypersurfaces and compared with various prescriptions (BY etc.) for hypersurface data. In the approach used, based on the perturbation formalism of Moncrief [12], the initial and evolved data was represented by a spacetime function ψ that is totally gauge invariant, so that the interpretation of the physics was not tainted by questions of coordinate choices.

The calculations were used to study a set of hypersurface data that somewhat generalize the BY data. Those sets considered were all conformally flat and longitudinal (CFL). In practice this gave, for each multipole of the perturbation, a complete set of differential equations that had to be satisfied by the hypersurface geometry and extrinsic curvature (or, in practice, ψ and its time derivative $\dot{\psi}$). The only remaining freedom is the choice of boundary conditions (consistent with asymptotic flatness). These choices are equivalent to the choice of conditions deep inside the throats representing the holes, i.e., in the asymptotically flat universes at the end of the throats away from “our” asymptotically flat universe. We focused on two choices of these boundary conditions. One choice was the choice of the BY data itself. The second was the choice that the solution at the horizon be “frozen” or “matched” to its initial value. This approach was based on the fact that very near the background horizon a simple analytic solution could be given for the evolution of the data on the initial hypersurface to subsequent hypersurfaces. The solution for ψ was simply that it was “frozen” to retain its initial value at the horizon. The solution for $\dot{\psi}$ reflected more detail, and was said to be “matched” to the initial solution at the horizon. We could also choose to have ψ “frozen,” but we could choose the boundary conditions for $\dot{\psi}$ to be the BY conditions, and so forth.

For a particle falling from rest at a large initial distance, we found that the solution that evolved, and the CFL data on later hypersurfaces were in serious disagreement. If evolved data were replaced by CFL data on a late hypersurface the resulting waveforms and radiated energies were drastically altered. We found furthermore: (i) In the class of CFL hypersurface data the best choice is the “frozen-matched” choice, but that the difference between this and other CFL choices is small compared to the disagreement with the evolved solution. (ii) The disagreement between evolved hypersurface data and CFL data does not lie, in any obvious way, in the “radiation content” of the data, but rather in the details of the data near the location of the particle. (iii) The disagreement between the true and CFL data was much more severe in $\dot{\psi}$ than in ψ .

In the present paper we look again at the problem of head on collision of two nonspinning holes in the particle limit, and ask whether there is a more successful alternative prescription for hypersurface data. More specifically, let us consider a configuration of black holes at late times that evolved from a precursor configuration at large separation, and let us suppose that we know the positions and momenta of the holes on the late time hypersurface. Is there a prescription for the data on the late hypersurface which is in good agreement with the “true” hypersurface data (i.e., the data evolved from the large-separation precursor), and which gives an accurate prediction of the radiated energy and waveform? The answer to this question seems to be that there is, and the prescription, at least in the particle limit, is a very simple one: that the data be “convective,” in a sense to be defined below.

In Sec. IIA we sketch the mathematics of the Moncrief formalism we use and of our notation and conventions, and we present some results of evolved data vs. CFL data; this sketch will be quite brief; a reader interested in the details will find them in Paper II. The proposal for convective data is discussed in general in Sec. IIB, and is implemented in a particular manner, for radial infall, in Sec. IIC. Numerical results from this implementation are given in Sec. IID. A discussion of the implications and possible extensions of this work is presented in Sec. III.

II. ASTROPHYSICAL INITIAL DATA

A. Review of particle results for BY initial data

1. Moncrief-Zerilli formalism

The numerical results we will present below will be for a particle infalling radially into a Schwarzschild black hole. Due to the axial symmetry of our problem, and the absence of rotation, the perturbations are pure even parity. To describe the perturbations, we use the Regge-Wheeler [13] notation, but not the Regge-Wheeler gauge. In this notation the even parity metric perturbations are decomposed into scalar, vector and tensor spherical harmonics, with coefficient functions $H_0^\ell, H_1^\ell, H_2^\ell, h_0^\ell, h_1^\ell, K^\ell, G^\ell$, depending on r, t the standard radial and time coordinates of the Schwarzschild background. For simplicity, we drop the multipole index ℓ on these perturbation functions.

The perturbation coefficients H_2, h_1, K, G describe only the perturbed 3-geometry, and are independent of the choice of shift and lapse. In terms of these, Moncrief [12] defines the totally gauge invariant function

$$\psi(r, t) = \frac{r}{\lambda + 1} \left[K + \frac{r - 2M}{\lambda r + 3M} \{H_2 - r\partial K/\partial r\} \right] + \frac{2}{r}(r - 2M) (r^2\partial G/\partial r - 2h_1) , \quad (2.1)$$

where we have used Zerilli's normalization for ψ and his notation

$$\lambda \equiv (\ell + 2)(\ell - 1)/2 . \quad (2.2)$$

The basic wave equation for an infalling particle is given in Paper I as

$$-\frac{\partial^2 \psi}{\partial t^2} + \frac{\partial^2 \psi}{\partial r^{*2}} - V_\ell(r)\psi = \mathcal{S}_\ell(r, t) . \quad (2.3)$$

Here $r^* \equiv r + 2M \ln(r/2M - 1)$ is the Regge-Wheeler [13] ‘‘tortoise’’ coordinate and V_ℓ is the Zerilli potential

$$V_\ell(r) = \left(1 - \frac{2M}{r}\right) \frac{2\lambda^2(\lambda + 1)r^3 + 6\lambda^2 M r^2 + 18\lambda M^2 r + 18M^3}{r^3(\lambda r + 3M)^2} . \quad (2.4)$$

The right hand side of Eq. (2.3) is a source term constructed from the particle stress energy [10,11]. For a point particle of proper mass m_0 , the stress energy is given by

$$T^{\mu\nu} = (m_0/U^0)U^\mu U^\nu \delta[r - r_p(t)]\delta^2[\Omega]/r^2 , \quad (2.5)$$

where U^μ is the particle 4-velocity, and $r_p(t)$ gives the radial position of the particle as a function of coordinate time, starting from $r_p = r_0$ at $t = 0$.

The total energy radiated in the ℓ th multipole, after a hypersurface at t_0 is

$$\text{Energy}_\ell = \frac{1}{64\pi} \frac{(\ell + 2)!}{(\ell - 2)!} \int_{t_0}^{\infty} (\dot{\psi}^\ell)^2 dt . \quad (2.6)$$

2. Functional freedom in the hypersurface data

An even parity multipole perturbation of the 3-geometry has the four functional (of r, t) degrees of freedom contained in h_1, H_2, K, G , but these must satisfy the (perturbed, multipole) Hamiltonian constraint, a single second order differential equation containing the particle source. The choice of a conformally flat 3-geometry reduces the problem to a single functional degree of freedom (since, in an appropriate coordinate system, $h_1 = G = 0$ and $H_2 = K$) satisfying the single Hamiltonian constraint. The only freedom is the choice of the constants specifying the homogeneous solution of the Hamiltonian constraint. One of those constants is fixed by the condition that the solution be well behaved at spatial infinity. The remaining constant can be specified to ‘‘freeze’’ the horizon value of ψ at its initial value, to make the solution inversion symmetric, or in other ways. If the requirement of conformal flatness is dropped, then any sufficiently smooth function can be added to a particular solution ψ that solves the Hamiltonian constraint.

For $\dot{\psi}$ things are a bit more complicated. For an even parity perturbative extrinsic curvature there are four functions of r, t , analogous to the four functions h_1, H_2, K, G specifying the 3-geometry perturbations. There are two second order equations, equivalent to $G_{tr} = 8\pi T_{tr}$ and $G_{t\theta} = 0$. If we require that the extrinsic curvature be longitudinal, then the extrinsic curvature must be derivable from a vector potential \vec{W} , and for a given even parity multipole the functional degrees of freedom are $W^r(t, r)$ and $W^\theta(t, r)$. Since these functions must satisfy two second order differential equations, we have no remaining functional freedom. We have only to choose the four constants that specify how much our solution contains of the four homogeneous solutions of the momentum constraints. Two of these constants are fixed by the requirement that the extrinsic geometry be well behaved at spatial infinity. The remaining two constants can be chosen to make the solution of the BY type, to make the solution ‘‘match’’ the initial solution at the horizon, etc. If the requirement of longitudinality is dropped, then any sufficiently smooth function can be added to any particular solution $\dot{\psi}$ of the momentum constraints.

3. Results for CFL hypersurface data

Here we briefly review the numerical results found for the CFL prescription. In the results presented here a particle started its infall from Schwarzschild radial coordinate $r_p = r_0 = 15(2M)$, where M is the mass of the spacetime (in the usual $c = G = 1$ units). At subsequent times, when the radial location r_p of the particle is smaller, and the time label of a $t =$ constant hypersurface is larger, we can extract the evolved ψ , replace it with a prescribed CFL ψ etc.

Figure 1 shows the result that is most important. At various times (parameterized by the particle location r_p^* at these times) the numerical evolution was stopped, and the evolved quadrupole ψ and $\dot{\psi}$ were replaced by the CFL prescribed data representing the particle position and momentum on this hypersurface. Evolution forward from this hypersurface is then done numerically. The resulting energy is then numerically computed. The true $\ell = 2$ energy for infall from $r_0 = 15(2M)$ is $0.0164(m_0^2/2M)$. If we evolve the prescribed data from a later surface we see that we get reasonably good agreement with the true energy for r_p^* larger than around $5(2M)$, corresponding to r_p around $4(2M)$. For smaller r_p the use of prescribed CFL data badly overestimates the radiated energy.

Comparisons of the true (i.e., evolved) quadrupolar $\psi, \dot{\psi}$ and the prescribed quadrupolar $\psi, \dot{\psi}$ are shown in the next two figures. Both are for a particle starting from rest at initial separation $r_0 = 15(2M)$ at $t = 0$. For both, the comparison is made at $t = 96.9(2M)$. This corresponds to the particle being at $r_p = 2(2M)$, and having momentum $P = 1.27m_0$. A comparison of ψ is given in Fig. 2 in which the solid curve shows the evolved ψ and the dashed curve is the CF ψ for a particle of mass m_0 , at location $r_p = 2(2M)$, with momentum $P = 1.27m_0$. The corresponding comparison for $\dot{\psi}$ is shown in Fig. 3. From these comparisons it appears that the CF solutions give a reasonably good approximation to ψ near the particle, but in the strong field region of the background, the CFL form of $\dot{\psi}$ has a very different shape near the particle than that of the evolved $\dot{\psi}$. We note here that the evolved $\dot{\psi}$ will, in general, have a $\delta[r - r_p]$ behavior at the location of the particle. This behavior is exactly included in both the CFL and the convective (see below) prescriptions.

B. Proposed astrophysical initial data

Suppose that our particle source starts at some position r_0, θ_0, φ_0 . On some later hypersurface, let us call it the $t = t_\Sigma$ hypersurface, suppose that we know the coordinate position x_p^j and the momentum P^j for the particle. (Here latin superscripts, j, k, \dots are spatial indices running from 1 to 3.) From the geodesic motion of the particle we can find x_p^j and P^j at any time t . Let us now take $\Psi(x^k; x_p^k)$ to be a form of ψ that is “appropriate” to the position (and momentum) of the particle. This could be, for example, the ψ corresponding to a CF 3-geometry for the particle. The next step is to promote this solution to a function of time, by putting in the explicit time dependence $x_p^k[t]$. (Note that the resulting time-dependent function $\Psi(x^k; x_p^k[t])$ is not based on a solution of Einstein’s equations, and will not solve the Zerilli equation.) Our proposal is to take the hypersurface data to be:

$$\psi|_{t_\Sigma} = \Psi(x^k; x_p^k[t_\Sigma]) \quad (2.7)$$

$$\dot{\psi}|_{t_\Sigma} = \left. \frac{\partial \Psi(x^k; x_p^k[t])}{\partial t} \right|_{t_\Sigma} = \left[\frac{dx_p^j[t]}{dt} \frac{\partial \Psi(x^k; x_p^k[t])}{\partial x_p^j} \right]_{t_\Sigma} . \quad (2.8)$$

With this choice we are, in effect, saying that ψ is changing in time only in order to adjust to the new particle position and momentum. The solution, in a sense, is dragged or transported to a new position. We call this the “convective” choice of $\dot{\psi}$.

Initial data, of course, must be chosen so that it solves the constraint equations. But here (so far) we have been discussing the choice only of the single gauge invariant function ψ on the hypersurface, and its time derivative. Since the constraints leave a functional degree of freedom in the initial 3-geometry and extrinsic curvature, ψ and $\dot{\psi}$ can be freely specified.

One motivation for this choice of hypersurface data is that the disagreement between evolved and prescribed initial data seems to be rooted in the CFL $\dot{\psi}$ much more than in ψ . The proposed convective choice of hypersurface data allows us to maintain the CF form of ψ , but find a new form of $\dot{\psi}$. A second motivation has to do with motion in which the hypersurface data is “obvious,” a particle in circular orbit at frequency Ω around a hole. In this case the appropriate approximation (neglecting radiation reaction to lowest order) is for the spacetime geometry to be periodic, with period $2\pi/\Omega$. More specifically, in terms of the coordinates t, r, θ, φ of the Schwarzschild (or Kerr) background, all spacetime functions should have the form $f(t, r, \theta, \varphi) = F(r, \theta, \varphi - \Omega t)$.

If we denote the position of the particle by $r_p = r_0, \theta_p = \pi/2, \varphi_p = \varphi_0 + \Omega t$. The solution for ψ must therefore have the functional form as

$$\psi(t, r, \theta, \varphi) = \Phi(r, \theta, \varphi - \Omega t) = \Phi(r, \theta, \varphi - \varphi_p[t] + \varphi_0) . \quad (2.9)$$

We can therefore take

$$\Psi(x^k; x_p^k[t]) = \Phi(r, \theta, \varphi - \varphi_p[t] + \varphi_0) . \quad (2.10)$$

This solution clearly obeys Eq. (2.8) on any hypersurface t_Σ , since the only time dependence in Ψ comes through its dependence on $\varphi_p[t]$. If on some hypersurface $t = t_\Sigma$, one chooses initial data

$$\psi|_{t_\Sigma} = \Phi|_{t_\Sigma}, \quad \dot{\psi}|_{t_\Sigma} = -\Omega \frac{\partial \Phi}{\partial \varphi} \Big|_{t_\Sigma}, \quad (2.11)$$

then, in principle, numerical evolution would give a purely periodic solution. For x^k, P^k corresponding to circular motion, one could, on the other hand, give other hypersurface data, such as CFL. The result would be a burst of initial radiation as the spacetime “settles down” to the periodic solution. If the circular orbit is meant to represent a late stage in a binary coalescence which is adiabatically decaying due to radiation reaction, then the periodic solution is obviously the appropriate one, and an initial burst of radiation is an anomaly due to the wrong choice of initial conditions.

C. Convective conformally flat data

We now apply the idea of convective $\dot{\psi}$ to a particle of mass m_0 falling radially into a Schwarzschild hole. As the appropriate form of ψ on a hypersurface we choose a conformally flat solution, with “frozen” horizon conditions. That is, on any hypersurface, the $r^* \rightarrow -\infty$ limit of ψ is the same as on the $t = 0$ hypersurface.

The meaning of this solution can be nicely described with the notation developed in Paper II. For even parity ℓ -pole perturbations of the 3-geometry, there are only two gauge invariant functions of r . One is the Moncrief ψ defined by Eq. (2.1). The second is I_{conf} , a gauge invariant measure of deviation of the 3-geometry from conformal flatness. (In the Regge-Wheeler [13] gauge $I_{\text{conf}} \equiv H_2 - K$.) For all CFL choices I_{conf} is zero on the hypersurface. This choice exhausts the functional freedom on the hypersurface, and the 3-geometry is then fixed by the Hamiltonian constraint. In practice this means that ψ satisfies a second-order differential equation in the r variable; the frozen horizon condition fixes the solution to that equation.

We are then choosing the same hypersurface ψ as a CFL choice. What is crucial is the difference in our choice of $\dot{\psi}$. Here our convective choice is tantamount to taking $\Psi[(x^k; x_p^k(t))]$ to be conformally flat for all t . This corresponds to a form of ψ , on each hypersurface, with $I_{\text{conf}} = 0$. It follows that

$$\dot{I}_{\text{conf}}|_{t_\Sigma} = 0. \quad (2.12)$$

In order to understand better the meaning of this condition it is useful to relate it to the Hamiltonian constraint. To derive this relationship conveniently we momentarily specialize to the gauge $h_0 = h_1 = G = 0$ of Regge and Wheeler [13]. In this gauge the Hamiltonian constraint is given by Zerilli [14] as his Eq. (C7a). For a particle at radial position r_p this takes the form

$$\left(1 - \frac{2M}{r}\right) \frac{\partial^2 K}{\partial r^2} + \left(3 - \frac{5M}{r}\right) \frac{1}{r} \frac{\partial K}{\partial r} - \frac{\lambda}{r^2} K - \frac{\lambda+2}{r^2} H_2 - \left(1 - \frac{2M}{r}\right) \frac{1}{r} \frac{\partial H_2}{\partial r} = -\kappa U^0 \left(1 - \frac{2M}{r}\right) \frac{1}{r^2} \delta[r - r_p], \quad (2.13)$$

where $\kappa = 2m_0 \sqrt{4\pi(2\ell+1)}$, m_0 is the mass of the particle, and U^0 is its time component of 4-velocity.

From Eq. (2.13) and its radial derivative, and from Eq. (2.1) we can write

$$I_{\text{conf}} = (r - 2M)\psi'' + \frac{[(\lambda - 3)r + 9M]M}{(\lambda r + 3M)r} \psi' - \frac{[27M^3 + 24\lambda M^2 r + 3\lambda(3\lambda + 1)Mr^2 + 2\lambda^2(\lambda + 1)r^3]}{(\lambda r + 3M)^2 r^2} \psi + \frac{\kappa U^0(1 - 2M/r)[\lambda(\lambda + 1)r^2 - 3M^2]}{(\lambda + 1)(\lambda r + 3M)^2} \delta[r - r_p] - \frac{\kappa U^0(r - 2M)^2}{(\lambda + 1)(\lambda r + 3M)} \delta'[r - r_p]. \quad (2.14)$$

This result was derived in the Regge-Wheeler gauge as an intermediate step, but is gauge-invariant. In a similar way, from the momentum constraints (see Eqs. (C7b), (C7d) of Zerilli [14]) and their r -derivatives, we obtain

$$\dot{I}_{\text{conf}} = (r - 2M)\dot{\psi}'' + \frac{[(\lambda - 3)r + 9M]M}{(\lambda r + 3M)r} \dot{\psi}' - \frac{[27M^3 + 24\lambda M^2 r + 3\lambda(3\lambda + 1)Mr^2 + 2\lambda^2(\lambda + 1)r^3]}{(\lambda r + 3M)^2 r^2} \dot{\psi} + \frac{2\kappa U^0 \dot{r}_p [9M^2 + 2M(\lambda - 3)r - \lambda(\lambda + 3)r^2]}{(\lambda + 1)r^2(\lambda r + 3M)^2} \delta[r - r_p] + \frac{\kappa U^0 \dot{r}_p (r - 2M)[9M^2 + 2M\lambda r - \lambda(\lambda + 1)r^2]}{(\lambda + 1)r(\lambda r + 3M)^2} \delta'[r - r_p] + \frac{\kappa U^0 \dot{r}_p (r - 2M)^2}{(\lambda + 1)(\lambda r + 3M)} \delta''[r - r_p]. \quad (2.15)$$

Note that this equation can be obtained as the time derivative of Eq. (2.14), but here we wish to emphasize its connection with the momentum constraints. The fact that there is consistency of the time derivative of the Hamiltonian constraint, and the spatial derivatives of the momentum constraints, is simply an expression of the fact that $G_0^\nu{}_{;\nu} = 0$.

We can view Eq. (2.14) as telling us that I_{conf} vanishes, since the right hand side vanishes for conformally flat data that satisfies the Hamiltonian constraint. Alternatively we can note that in Eq. (2.14) if we put I_{conf} to zero, what results is a second order radial differential equation for ψ . In this sense, the condition $I_{\text{conf}} = 0$ and the Hamiltonian constraint gives us (aside from boundary conditions) the initial value of ψ . In the same manner we can note that $\dot{I}_{\text{conf}} = 0$ in Eq. (2.15) gives us a radial differential equation for $\dot{\psi}$. From this point of view the condition $\dot{I}_{\text{conf}} = 0$ and the momentum constraints are fixing the form of $\dot{\psi}$. By contrast, in the CFL prescription, the form of $\dot{\psi}$ is fixed by the momentum constraints and the condition of longitudinality, roughly the condition that the conformal part of the extrinsic curvature can be derived from a vector potential.

To see how our proposal works, let us first consider the radial infall of a particle into a Schwarzschild hole. We have seen in Paper II that there is a preferred choice, ψ_f , that keeps its value at the event horizon ‘‘frozen’’

$$\psi_f = \frac{2m(r_p)}{\lambda+1} \frac{\sqrt{4\pi/(2\ell+1)}}{\lambda r + 3M} r \sqrt{r/\bar{r}} \times \left[\left(\lambda + 1 + \frac{M}{r} + \sqrt{1-2M/r} \left(\ell + \sqrt{\bar{r}/r} \right) \right) \Gamma_{\text{hom}}(r_p) \frac{(M/2)^{2\ell+1}}{\bar{r}_p^{\ell+1} \bar{r}^\ell} + \left\{ \begin{array}{l} \left(\lambda + 1 + M/r + \sqrt{1-2M/r} \left(\ell + \sqrt{\bar{r}/r} \right) \right) (\bar{r}_p/\bar{r})^\ell \\ \left(\lambda + 1 + M/r + \sqrt{1-2M/r} \left(\sqrt{\bar{r}/r} - \ell - 1 \right) \right) (\bar{r}/\bar{r}_p)^{\ell+1} \end{array} \right\} \right], \quad (2.16)$$

where

$$\bar{r} \equiv \left(\sqrt{r} + \sqrt{r-2M} \right)^2 / 4, \quad (2.17)$$

and where the upper expressions apply in the case $\bar{r} > \bar{r}_p$, and the lower for $\bar{r} < \bar{r}_p$. Here, as in Paper II

$$\Gamma_{\text{hom}}(\bar{r}_p) = \frac{m(r_0)}{m(r_p)} \left(\frac{\bar{r}_p}{\bar{r}_0} \right)^{\ell+1} (1 + \Gamma_{\text{hom}}(r_0)) - 1, \quad (2.18)$$

where $\Gamma_{\text{hom}}(r_0)$ represents the arbitrariness in choosing the data on the initial hypersurface $t = 0$ (when the particle started at rest and was located at $r_p = r_0$), and

$$m(r_p) = \frac{1}{2} m_0 \left(1 + \frac{1}{\sqrt{1-2M/r_p}} \right) \epsilon_0. \quad (2.19)$$

where $\epsilon_0 = \sqrt{1-2M/r_0}$ for a particle starting at rest when $r = r_0$, and $\epsilon_0 = 1/\sqrt{1-v_\infty^2}$ for a particle with velocity v_∞ at infinity, and $U^0 = \epsilon_0/(1-2M/r_p)$.

From this expressions we compute the ‘‘convective’’ $\dot{\psi}_c = \dot{r}_p \partial_{r_p} \psi_f$

$$\dot{\psi}_c = \frac{2m(r_p) \sqrt{4\pi/(2\ell+1)}}{\lambda+1} \frac{r \sqrt{r/\bar{r}}}{\lambda r + 3M} \frac{\dot{r}_p}{(r_p - 2M)} \times \left[\left(\lambda + 1 + \frac{M}{r} + \sqrt{1-2M/r} \left(\ell + \sqrt{\bar{r}/r} \right) \right) \left((\ell+1) \sqrt{1-2M/r_p} + M/(r_p + r_p \sqrt{1-2M/r_p}) \right) \frac{(M/2)^{2\ell+1}}{\bar{r}_p^{\ell+1} \bar{r}^\ell} + \left\{ \begin{array}{l} \left(\lambda + 1 + M/r + \sqrt{1-2M/r} \left(\ell + \sqrt{\bar{r}/r} \right) \right) \left(\ell \sqrt{1-2M/r_p} - M/(r_p + r_p \sqrt{1-2M/r_p}) \right) (\bar{r}_p/\bar{r})^\ell \\ - \left(\lambda + 1 + M/r + \sqrt{1-2M/r} \left(\sqrt{\bar{r}/r} - \ell - 1 \right) \right) \left((\ell+1) \sqrt{1-2M/r_p} + M/(r_p + r_p \sqrt{1-2M/r_p}) \right) (\bar{r}/\bar{r}_p)^{\ell+1} \end{array} \right\} \right], \quad (2.20)$$

where the upper expressions apply in the case $\bar{r} > \bar{r}_p$, and the lower for $\bar{r} < \bar{r}_p$. For radial infall $\dot{r}_p = -(1-2M/r_p) \sqrt{2M/r_p + \epsilon_0^2 - 1} / \epsilon_0$. Note that the choice of the freezing condition for ψ_f ensures that $\dot{\psi}_c$ vanishes on the horizon. This would not be true if we had taken either the particle limit of the Misner [15] or Brill-Lindquist [16] solutions for ψ . It is also worth stressing that $\dot{\psi}_c$ does not depend on $\Gamma_{\text{hom}}(r_0)$.

In principle, it could turn out that the CFL prescription and the convective prescription are the same. In Fig. 4 we show that this is not the case. This figure shows \dot{I}_{conf} for a particle dropped from rest at $r_0 = 15(2M)$. For the $t = 0$ hypersurface, with the particle at $r_p = 15(2M)$ (equivalent to $r_p^* = 17.64(2M)$), the solution is momentarily stationary, and hence I_{conf} is momentarily stationary, that is, $\dot{I}_{\text{conf}} = 0$. Plots are given of \dot{I}_{conf} on hypersurfaces a short time after the initial hypersurface, constant- t hypersurfaces corresponding to particle positions $r_p^* = 14.55(2M)$ and $r_p^* = 11.15(2M)$. The figure shows clearly that \dot{I}_{conf} does not vanish.

D. Numerical results

For some purposes the most important question to ask about a prescription for late time hypersurface data is whether it leads to a reasonably accurate estimate of the radiated gravitational wave energy that is generated in an astrophysical event. For the problem of a particle falling in from rest at r_0 , at time $t = 0$, we know with considerable accuracy the energy radiated in each multipole during the infall. We now must ask: if we replace the evolved data on a late hypersurface by some prescription (CFL, convective, . . .), what radiated energy will we calculate? A numerical answer to this question is shown in Fig. 5. For a particle falling from $r_0 = 15(2M)$, the “true” quadrupole gravitational radiation emitted is $1.64 \times 10^{-2} m_0^2 / (2M)$. Figure 5 shows the radiation that is computed if the evolved data on a hypersurface is replaced with prescribed data and evolved forward in time. The prescribed data used for the 3-geometry is conformally flat with a frozen horizon boundary condition. The value of $\dot{\psi}$ is given by the convective prescription. The results show that the use of such prescribed data, even at fairly late times, gives a very good approximation to the radiated energy. The worst case is an overestimate of the energy by a factor of around 2.4. This is to be contrasted with energy computed for prescribed CFL data, shown in Fig. 1, where the error grows without bound as the hypersurface is taken to late times. The result is significantly in error only for data prescribed on a hypersurface when the particle radial position r_p is around the peak of the Zerilli potential in Eq. (2.4), where we would expect the largest deviations in results based on any simple prescription. To clarify the relationship of the Zerilli potential and errors in the computed energy, the Zerilli potential is also indicated in Fig. 5.

The success of the new prescription is demonstrated in Figs. 6 and 7. These figures compare the new prescription (conformally flat, frozen-horizon, convective) for hypersurface data with the true (i.e., evolved) data and with the BY data, on several hypersurfaces. In Figs. 6–7 we use BY data as our example of the CFL prescription, since BY is the most familiar case. There would be negligible differences in appearance if we used instead any of the other CFL variations studied in Paper II.

Figure 6 shows $\partial\psi/\partial t$ for a particle falling from rest from position $r_0 = 1.5(2M)$ at time $t = 0$. This is not a reasonable astrophysical scenario, but it serves to emphasize strong field effects and magnify differences in hypersurface data. The improvement of the new prescription over BY data is dramatic, even on a hypersurface ($t = 2.2[2M]$, $r_p = 1.34[2M]$) soon after the initial hypersurface. The new prescription agrees very well with the evolved data, both in its general shape near the particle, and in its numerical values; by contrast the BY data disagrees sharply with the evolved data. This disagreement grows at later times, and at $t = 4.5(2M)$ the BY and evolved curves have little similarity. On the other hand, the new prescription gives a curve that agrees qualitatively with the true data, and agrees in size within a factor of two. The same comparison is made in Figs. 7 for a particle falling from rest at $r_0 = 15(2M)$ at $t = 0$. Here we see that both the new prescription and BY data agree with the evolved data reasonably well until the particle approaches the strong field region near the peak of the Zerilli potential. At smaller radii there are significant quantitative differences between the data of the new prescription and the evolved data, but these differences are much milder than the wide divergence of the BY data from the evolved data.

A comparison of outgoing waveforms appears in Figs. 8. The solid curves in both (a) and (b) show the true waveform, seen by an observer at $r_{\text{obs}} = 1000(2M)$, for the quadrupolar part of ψ , for a particle falling from rest, at time $t = 0$ from position $r_p = 15(2M)$ (equivalent to $r_p = 17.64[2M]$). The dotted curve in (a) shows the outgoing waveform that results if conformally flat, frozen-horizon, convective data is substituted for true data on the $t = 63.9(2M)$ hypersurface. Similarly the dashed curve in (a) shows the waveform if the substitution is made at $t = 93.5(2M)$. The three curves show remarkable agreement after the start of quasinormal ringing. Only at early times is there a noticeable difference: the long shallow dip in the true waveform is reduced or missing from the waveforms generated by the data of the new prescription. The dotted curve in (b) shows a waveform comparison at a yet later time. Although the new waveform has roughly the same magnitude of quasinormal ringing as the true waveform, it has a large phase shift relative to the true curve. This can be understood with the idea that quasinormal ringing is generated near the peak of the curvature potential. For the dotted curve in (b), the particle is placed at a smaller radius than the potential peak, and has no history of having moved inward through the potential peak. The quasinormal ringing excited by the prescribed data, then, must start at the time of the hypersurface on which prescribed data is defined. For the true curve, the quasinormal ringing starts earlier, at the time the particle passed going inward. Numerical experiments confirm with reasonable accuracy that the phase shift depends on particle position in this manner.

In the work of Abrahams and Cook [17], and Baker and Li [18], the “close limit” was used to evolve prescribed data for the head on collision of equal mass holes. The close limit approximation applies to a hypersurface late enough that a single horizon surrounds both colliding holes, and only the large radius fields of the colliding holes are of importance. We have seen in Paper II, however, that in the particle limit this close limit does not work at *any* separation of the holes, if BY prescribed data is used. The method fails at large separation, because the close limit conditions fail; the method fails at small separation because the BY data is a bad representation of the true data. In Fig. 9 we see that the close limit does work at sufficiently small separations if the new prescription (conformally flat, horizon frozen,

convective) is used.

III. CONCLUSIONS

We have seen that the convective prescription for initial data for a black hole coalescence gives a much better description of the way in which hypersurface data evolves than does the CFL prescription. The demonstration, however, has been confined to an example of a coalescence which (i) was a head on collision (ii) used a conformally flat 3-geometry, and (iii) involved the particle limit of nonrotating holes.

It will be relatively simple to study another particle-limit example that is free of the first two of these limitations. As already mentioned in Sec. IIB, the steady state solution for a particle in circular orbit around a hole is an example of a solution that is convective for any time slice. It is straightforward to find this convective periodic solution in the form of a Fourier series, and this solution will not be conformally flat. This opens the possibility for several interesting comparisons. It will be reasonably straightforward to start with CFL data for a particle which at one instant has the correct position and momentum for a circular orbit. Similarly, it is simple to find initial conditions corresponding to a convective, initially conformally flat data. Both these solutions could be evolved forward in time and the anomalous radiation could be found that is emitted as the field settles into its steady state solution. The amount of radiation energy in this anomalous initial burst is an indicator of how sensitive conclusions will be to the details of the initial data prescribed. If the energy is significant compared to the steady state emission during a single orbit, it is a sign that CFL initial data will give misleading results for black hole coalescence, at least for coalescing holes of very different mass.

A considerably more difficult issue is the particle-limit context of our development. How are these ideas to be applied to coalescence of holes of comparable mass? In a very general way one might try to use the idea of a time sequence of 3-geometries in order to fix the initial extrinsic curvature. There are many caveats that go with such a proposal, along with the question of just how one implements such a scheme? One could, for example, add time dependence to the conformal factor with the convective description, by making the parameters (location and momentum of the holes) time dependent. But we do not know at the outset what the correct dynamical sequence is for strong field motion. There is a more serious difficulty. Such a scheme would give a definitive prescription for finding the time derivatives of the 3-geometries, and (with some physically motivated choice of lapse and shift) would give us the initial extrinsic curvature. This extrinsic curvature should in general give a result that does not satisfy the momentum constraint.

A more promising approach might be to try to generalize the condition $\dot{I}_{\text{conf}} = 0$. One might, for example, use the Cotton-York [19] tensor β_{ij} , which vanishes if and only if the 3-geometry is conformally flat. By setting the time derivative of this tensor to zero one would capture, in the nonlinear theory, the same condition as $\dot{I}_{\text{conf}} = 0$ in perturbation theory. A scheme like this, however, is based on conformal flatness, and this raises the question of whether conformal flatness itself should be retained in an astrophysically motivated specification of initial data.

Somewhat related to the question of a convective prescription, but somewhat independent, is the question of the frozen horizon condition. For representing initial data that evolved from an earlier astrophysical configuration, the frozen horizon condition is “obviously” a correct constraint on data on a late hypersurface. Whether or not the convective prescription is used in connection with numerical relativity, the frozen horizon condition should be used if one wants a representation of an astrophysical problem.

ACKNOWLEDGMENTS

This work has been partially supported by the National Science Foundation under grant PHY0507719.

-
- [1] L. S. Finn in Proceedings of GR14, edited by M.Fancaviglia et al. (World Scientific, Singapore, 1997) p. 147.
 - [2] B.F. Schutz, preprint AEI-033.
 - [3] É.É. Flanagan and S.A. Hughes, preprint gr-qc 9701039.
 - [4] For example, J. W. York, Jr. and T. Piran, *Spacetime and Geometry*, edited by R. Matzner and L. Shepley (Univ. of Texas Press, Austin, 1982), pp. 147 – 176, and references therein.
 - [5] J. W. York, Jr., *J. Math. Phys.* **14**, 456 (1973).
 - [6] J. M. Bowen and J. W. York, Jr., *Phys. Rev.* **D21**, 2047 (1980).

- [7] J. D. Rauber in *Dynamical Spacetimes and Numerical Relativity*, edited by J. M. Centrella (Cambridge Univ. Press, Cambridge, 1986), p. 304.
- [8] G. B. Cook, Phys. Rev. **D44**, 2983 (1991).
- [9] R. Gleiser, O. Nicasio, R. Price, J. Pullin. In preparation.
- [10] C. O. Lousto and R. H. Price, Phys. Rev. **D55**, 2124, (1997) (Paper I).
- [11] C. O. Lousto and R. H. Price, to appear in Phys. Rev. **D56** (1997) (Paper II).
- [12] V. Moncrief, Ann. Phys. (NY) **88**, 323 (1974).
- [13] T. Regge and J. A. Wheeler, Phys. Rev. **108**, 1063 (1957).
- [14] F. J. Zerilli, Phys. Rev. **D2** 2141 (1970).
- [15] C. W. Misner, Ann. of Phys. **24**, 102 (1963); R. W. Lindquist, J. Math. Phys. **4**, 938 (1963).
- [16] D. R. Brill and R. W. Lindquist, Phys. Rev. **131**, 471 (1964).
- [17] A. M. Abrahams and G. B. Cook, Phys. Rev. **D50**, R2364 (1994).
- [18] J. Baker and C. B. Li, Class. Q. Grav. **14**, L77 (1997).
- [19] J. W. York, Jr., Phys. Rev. Lett. **26**, 1656 (1971).

FIG. 1. Radiated energy for replacement of evolved data by prescribed data. The specific prescribed data used was (CFL) conformally flat, longitudinal data with ψ at the horizon taken to be “frozen” to the starting value, and $\dot{\psi}$ “matched” to the starting form. A particle was started from rest at $r_0 = 15(2M)$ with momentarily stationary data, and the solution for ψ was evolved numerically. On various constant time hypersurfaces, labeled with the r_p^* position of the particle on the hypersurface, the evolved data was replaced by the frozen-matched prescribed data, and evolved forward. The radiated $\ell = 2$ energy is plotted as a function of the hypersurface label r_p^* at which the replacement was made.

FIG. 2. Comparison of evolved and prescribed ψ for infall from rest at $r_0 = 15(2M)$ at $t = 0$. The comparison is shown for the hypersurface at $t = 96.9(2M)$, at which time the particle has fallen to $r_p = 2(2M)$ and has a momentum $P = 1.27m_0$. The prescribed ψ shown is for CF 3-geometry, with a frozen boundary condition at the horizon.

FIG. 3. Comparison of evolved and prescribed $\dot{\psi}$ for infall from rest at $r_0 = 15(2M)$ at $t = 0$. The comparison is shown for the hypersurface at $t = 96.9(2M)$, at which time the particle has fallen to $r_p = 2(2M)$ and has a momentum $P = 1.27m_0$. The prescribed $\dot{\psi}$ shown is for CFL extrinsic curvature with the boundary condition at the horizon “matched” to the conditions at $t = 0$.

FIG. 4. The time derivative of the index of conformality \dot{I}_{conf} for the CFL prescription applied on constant- t hypersurfaces, for a particle that starts from rest at $r_p^* = 17.64(2M)$ [$r_p = 15(2M)$]. The figure shows that the CFL prescription, in contrast to the convective prescription, implies a nonvanishing \dot{I}_{conf} .

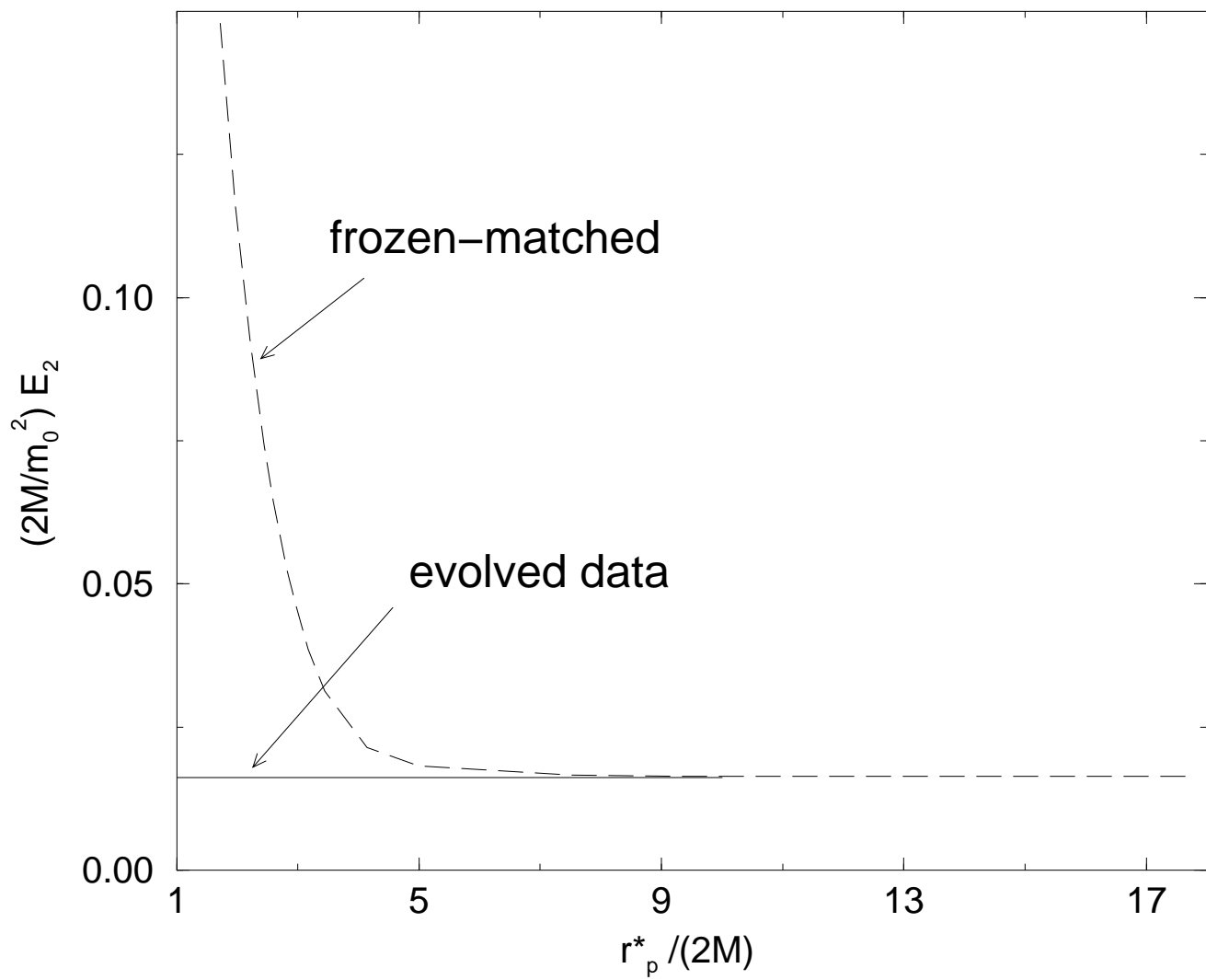
FIG. 5. Radiated quadrupole energy for a particle falling from rest at $r_0 = 15(2M)$. The energy actually radiated (labeled “True energy” is the horizontal line at $E_2 = 1.64 \times 10^{-2} m_0^2 / (2M)$). The dashed line shows energy computed from convective, conformally flat, horizon frozen boundary conditions. The prescribed data was used for a hypersurface on which the particle was at position r_p^* , and evolved forward in time. To underscore the role of the Zerilli potential, a scaled plot of the potential is shown as a dotted curve. This plot of the potential is shifted vertically so that aligns with the energy curve as $r^* \rightarrow \infty$.

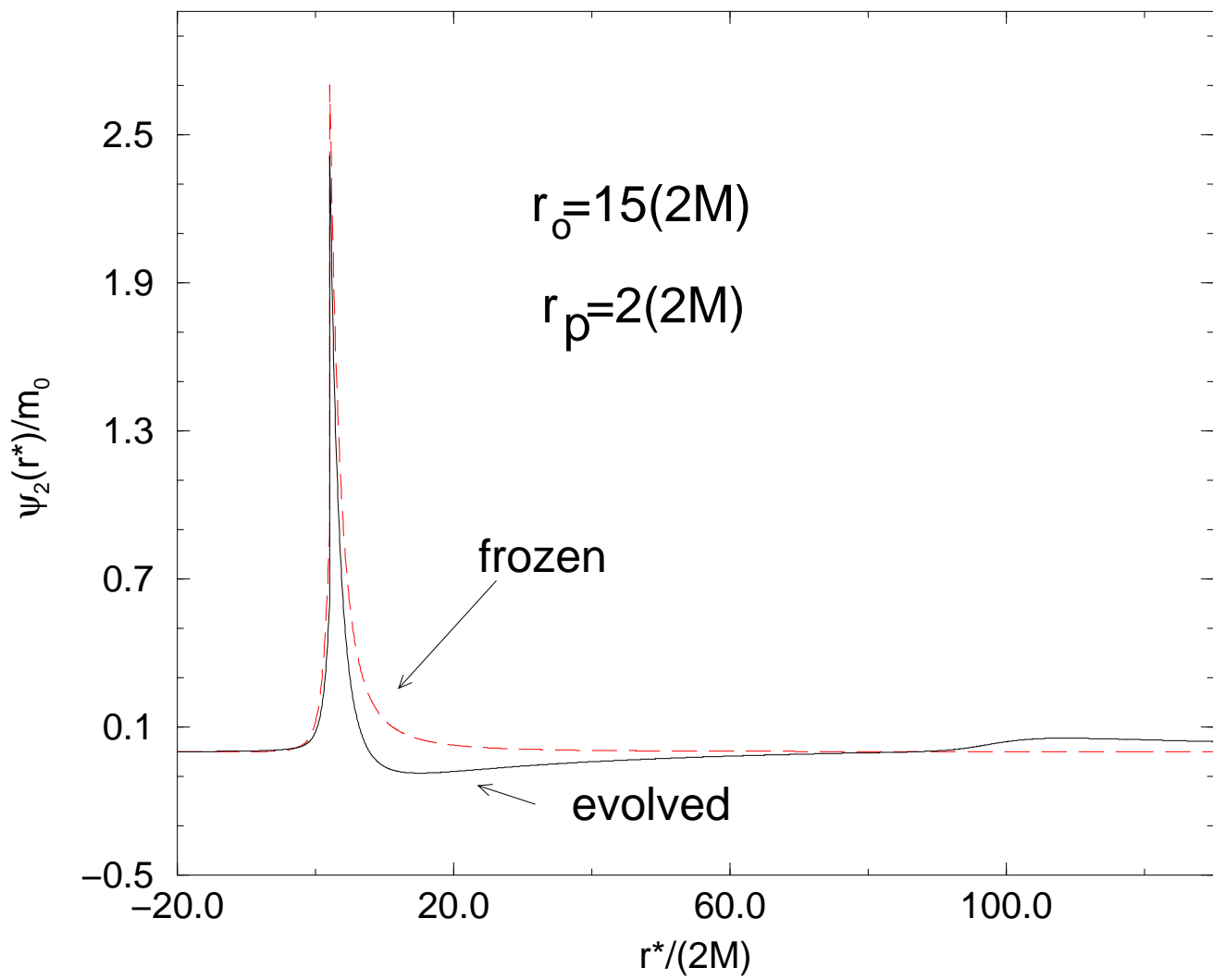
FIG. 6. Comparison of the evolved $\dot{\psi}$ with the new prescription (conformally flat, frozen-horizon, convective) and with BY data, on three successive hypersurfaces, for a particle started from rest at $r_0 = 1.5(2M)$. Even at very early stages the BY prescription fails. By contrast, the new prescription continues to give good predictions for most of the trajectory.

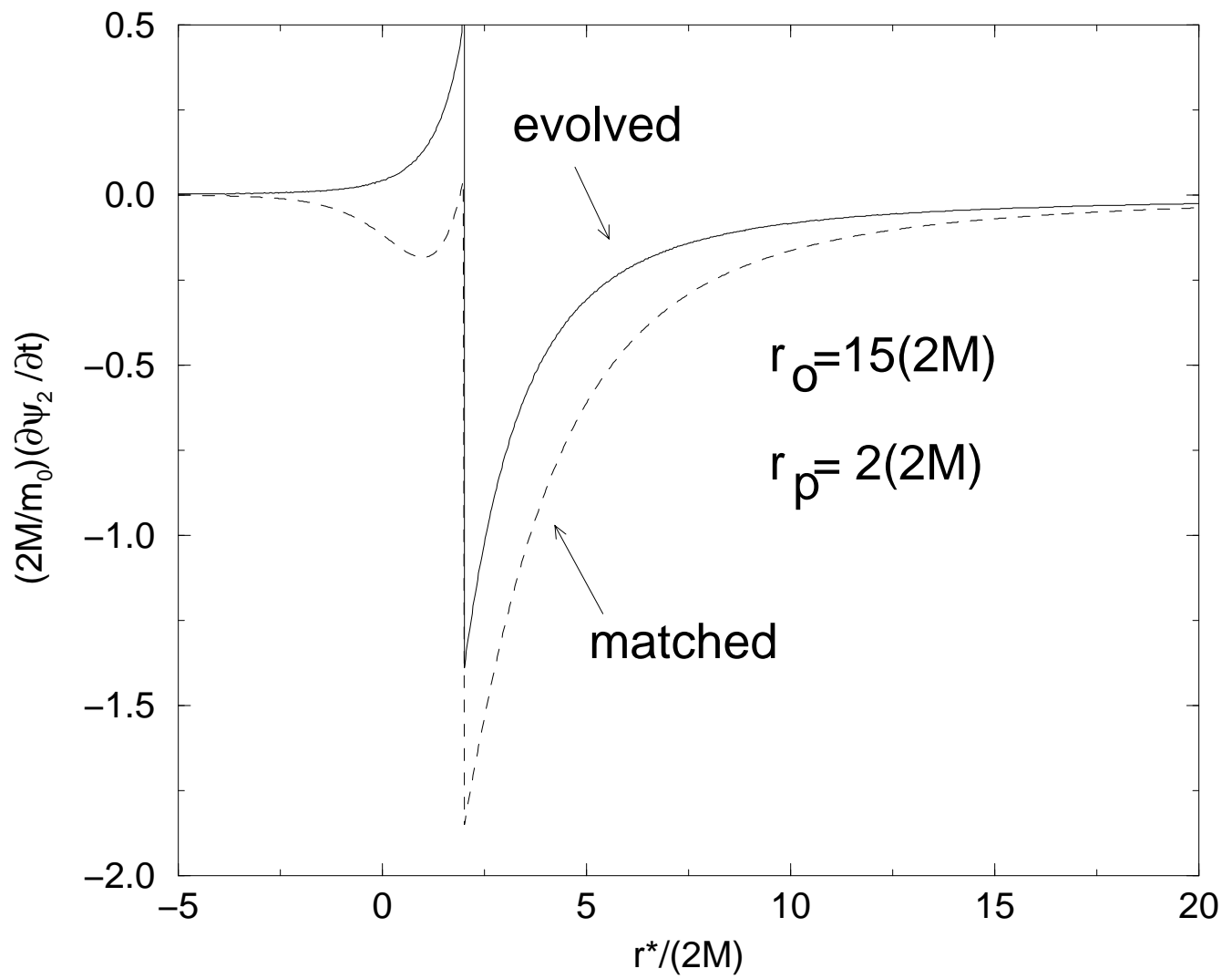
FIG. 7. Comparison of the evolved $\dot{\psi}$ with the new prescription (conformally flat, frozen-horizon, convective) and with BY data, on three successive hypersurfaces, for a particle started from rest at $r_0 = 15(2M)$. At very early stages the BY and new prescriptions give reasonable accuracy. At somewhat later times BY predictions are greatly in error, while the new prescription continues to give good predictions for most of the trajectory outside the peak of the potential.

FIG. 8. The waveform as seen by an observer located at $1000(2M)$. The solid line is the waveform generated by the infall of a particle from rest at $r_0 = 15(2M)$. The other curves are the result of replacing the evolved data with new data (conformally flat, frozen-horizon, convective) on hypersurfaces at the times indicated. If the replacement is made early enough (before the particle reaches the maximum of the Zerilli potential) the excitation of quasinormal ringing has the correct magnitude and phase, as can be seen in (a). For a replacement at a later time, shown in (b), there is a shift in the quasinormal ringing.

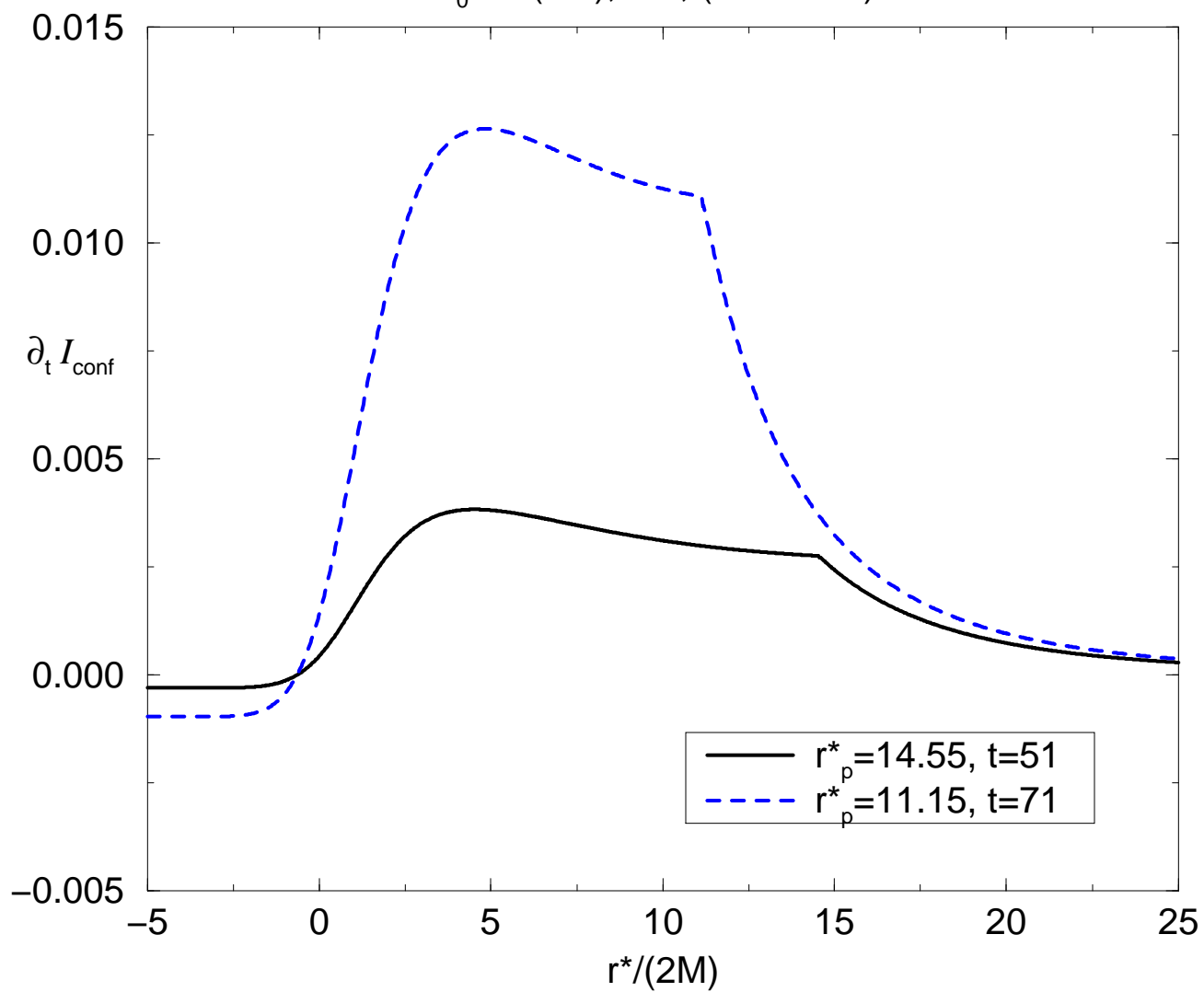
FIG. 9. The $\ell = 2$ radiated energy as predicted by the extension of the close limit (Ref. [18]) to the particle case. Quadrupolar energy calculated from the close limit, applied to the new prescription for data on hypersurfaces at various particle position r_p^* , are compared with the true radiated energy. These close limit results are reasonably accurate at sufficiently small separation. This should be contrasted with the situation for CFL data, given in Fig. 26 of Paper II, where disagreement was divergent at small separation



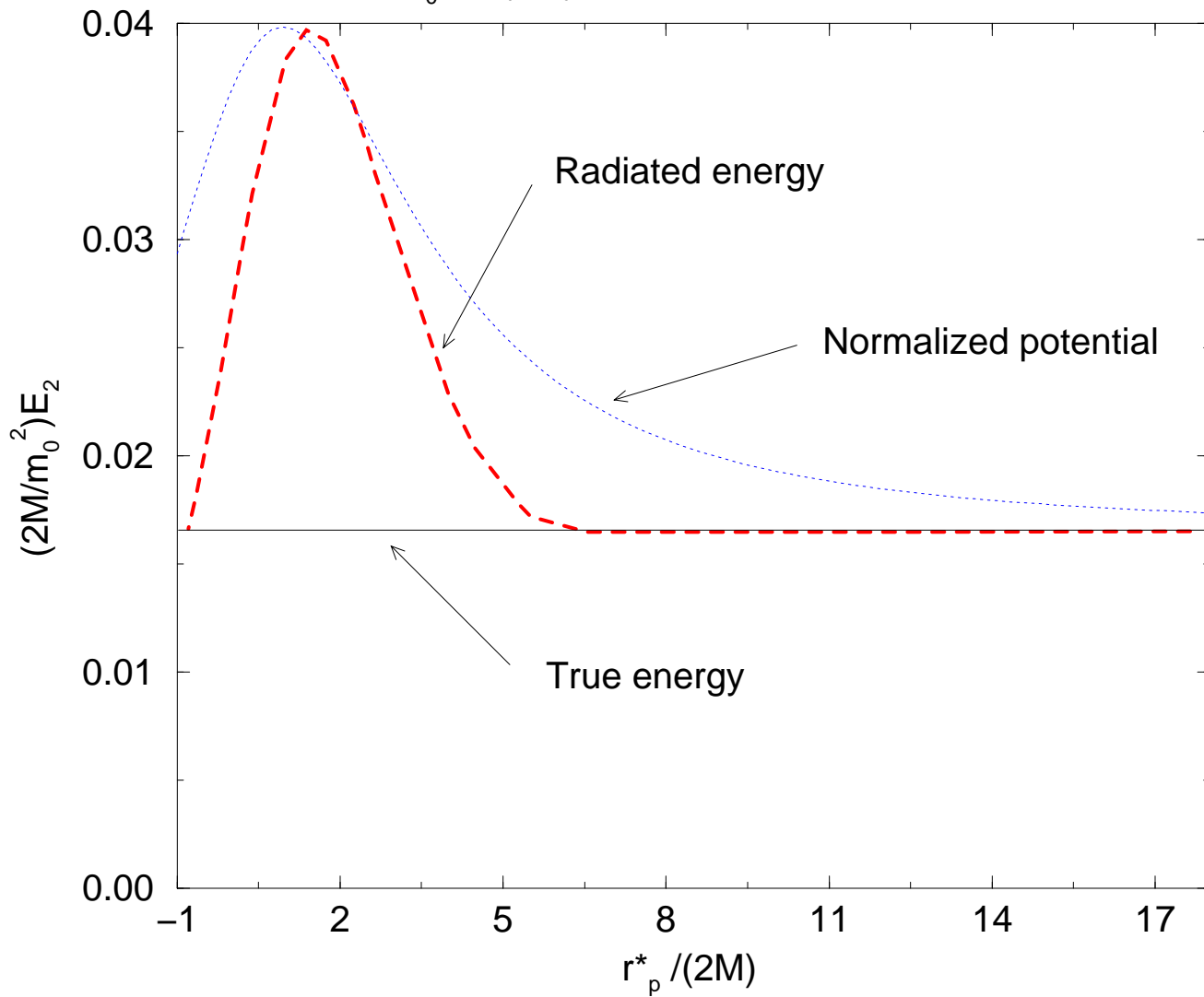




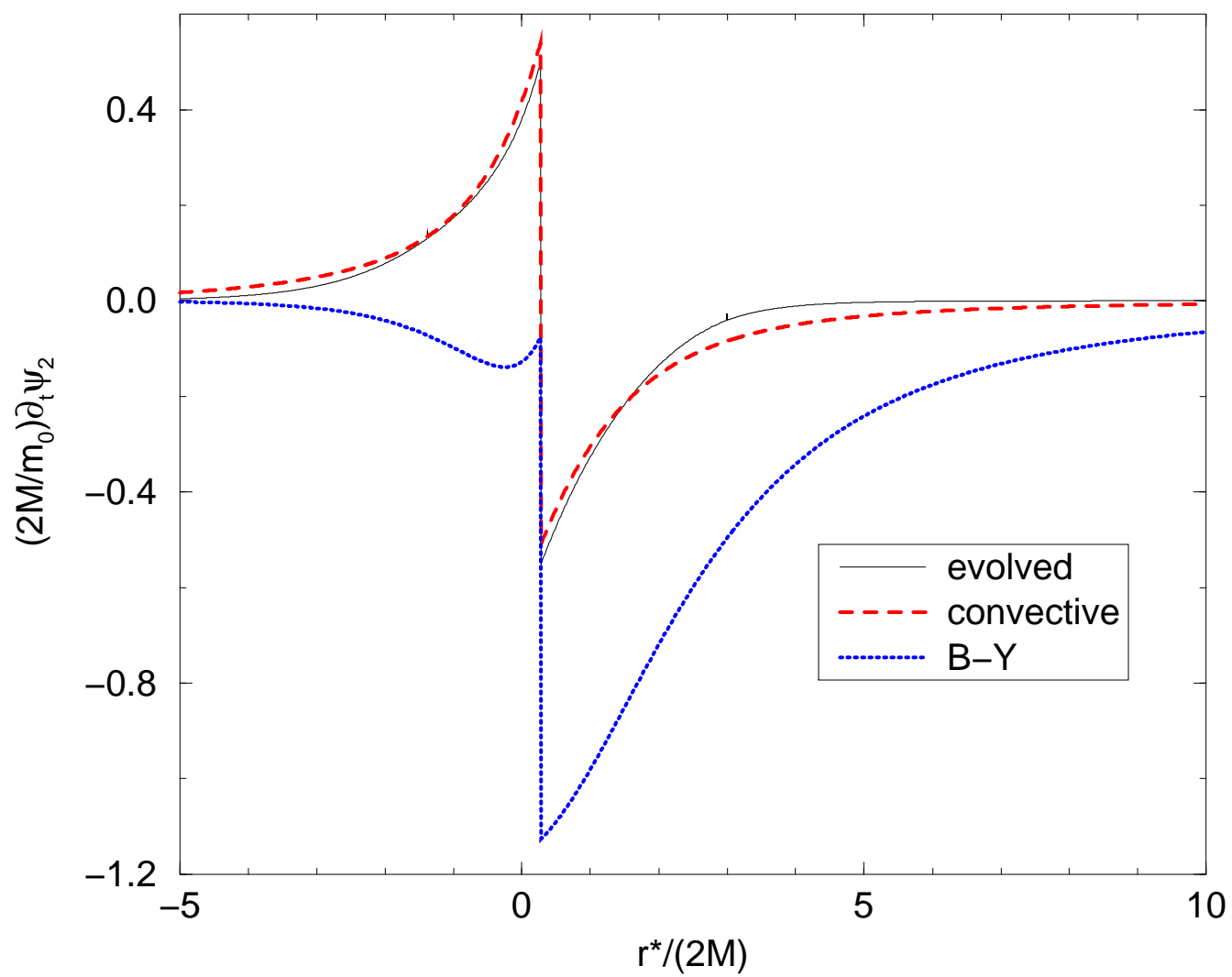
$r_0=15(2M), l=2, (\text{CFL data})$



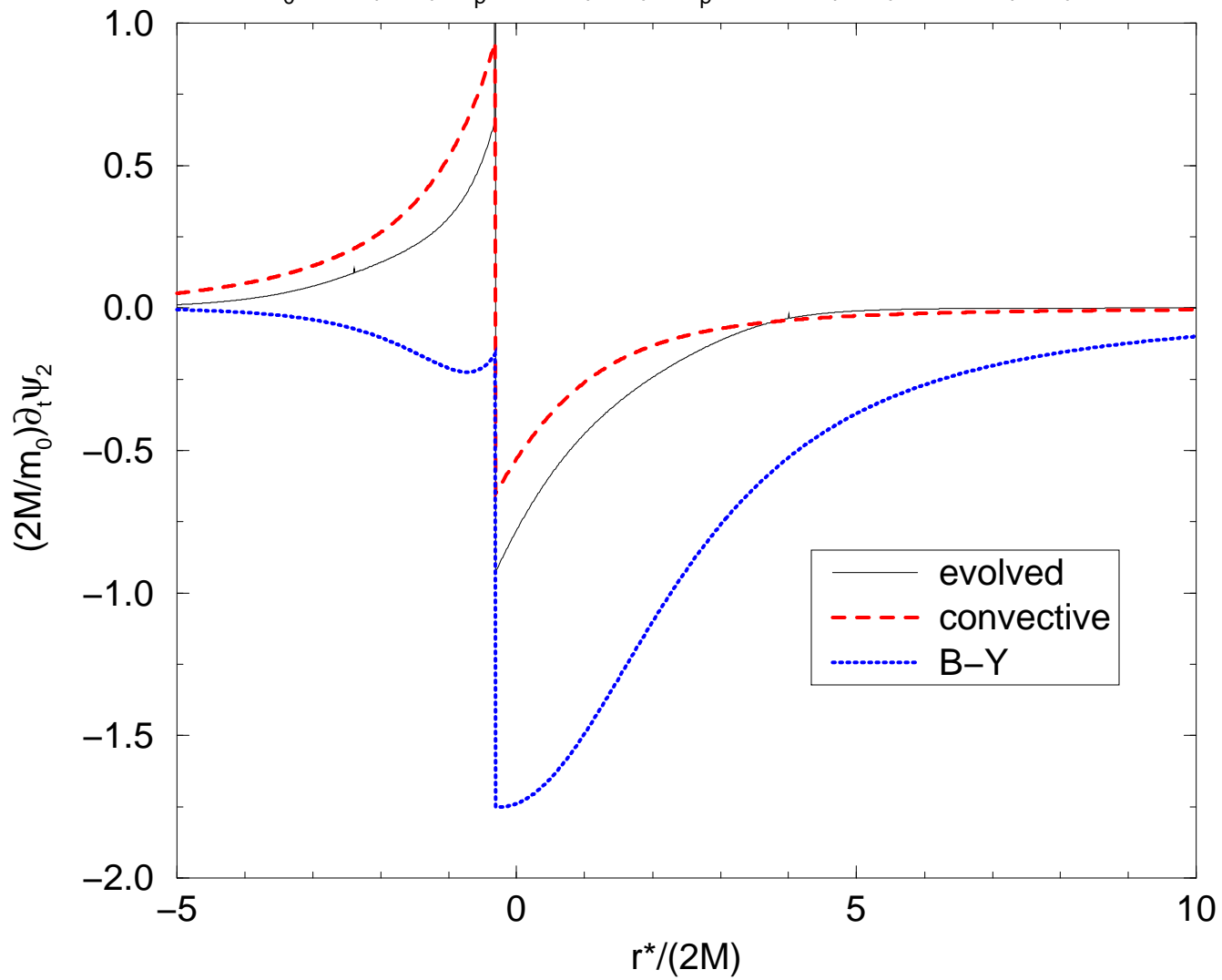
$r_0=15(2M), l=2, \text{ frozen-convective}$



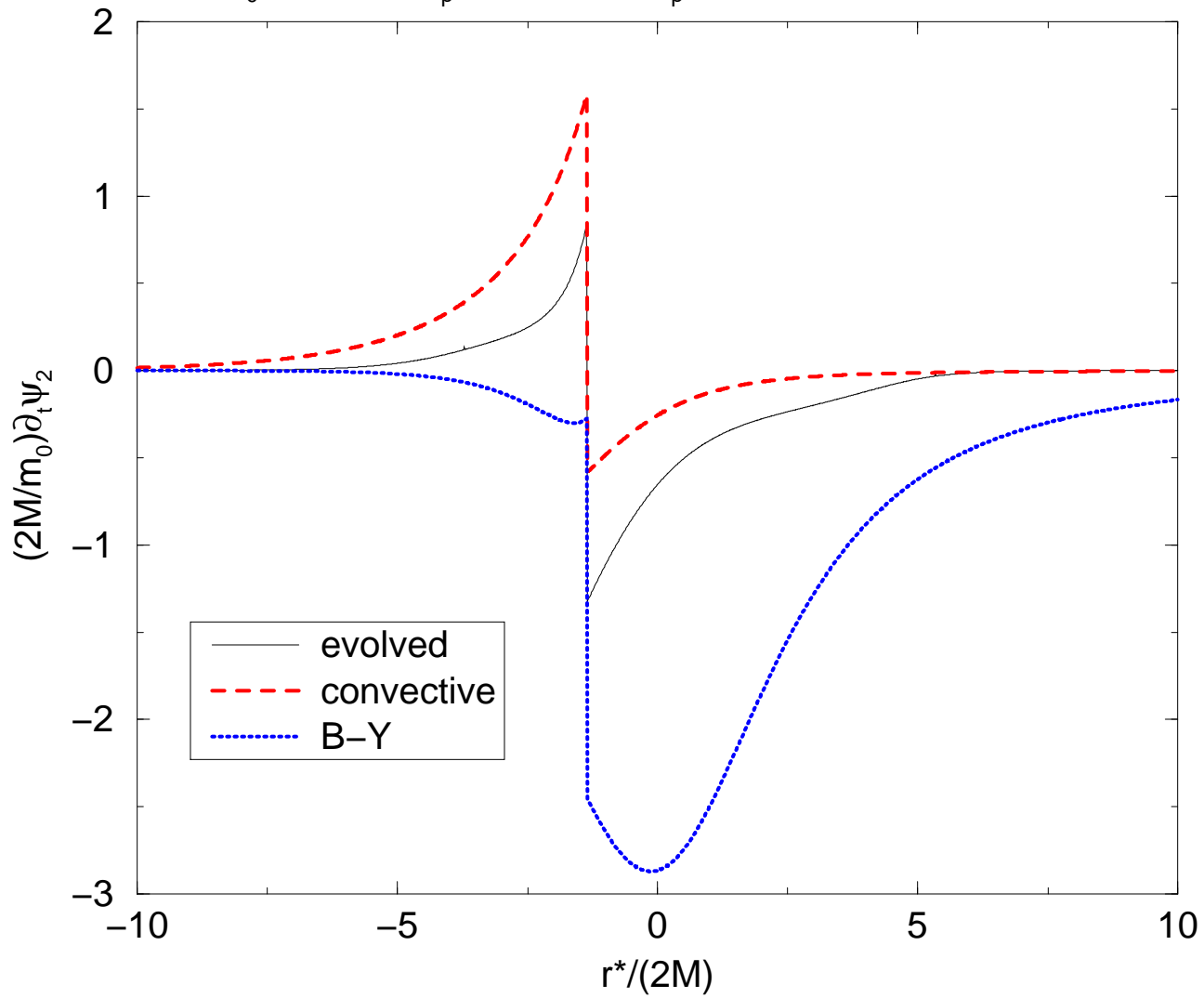
$r_0=1.5(2M)$, $r_p=1.34(2M)$, $r_p^*=0.28(2M)$, $t=2.2(2M)$



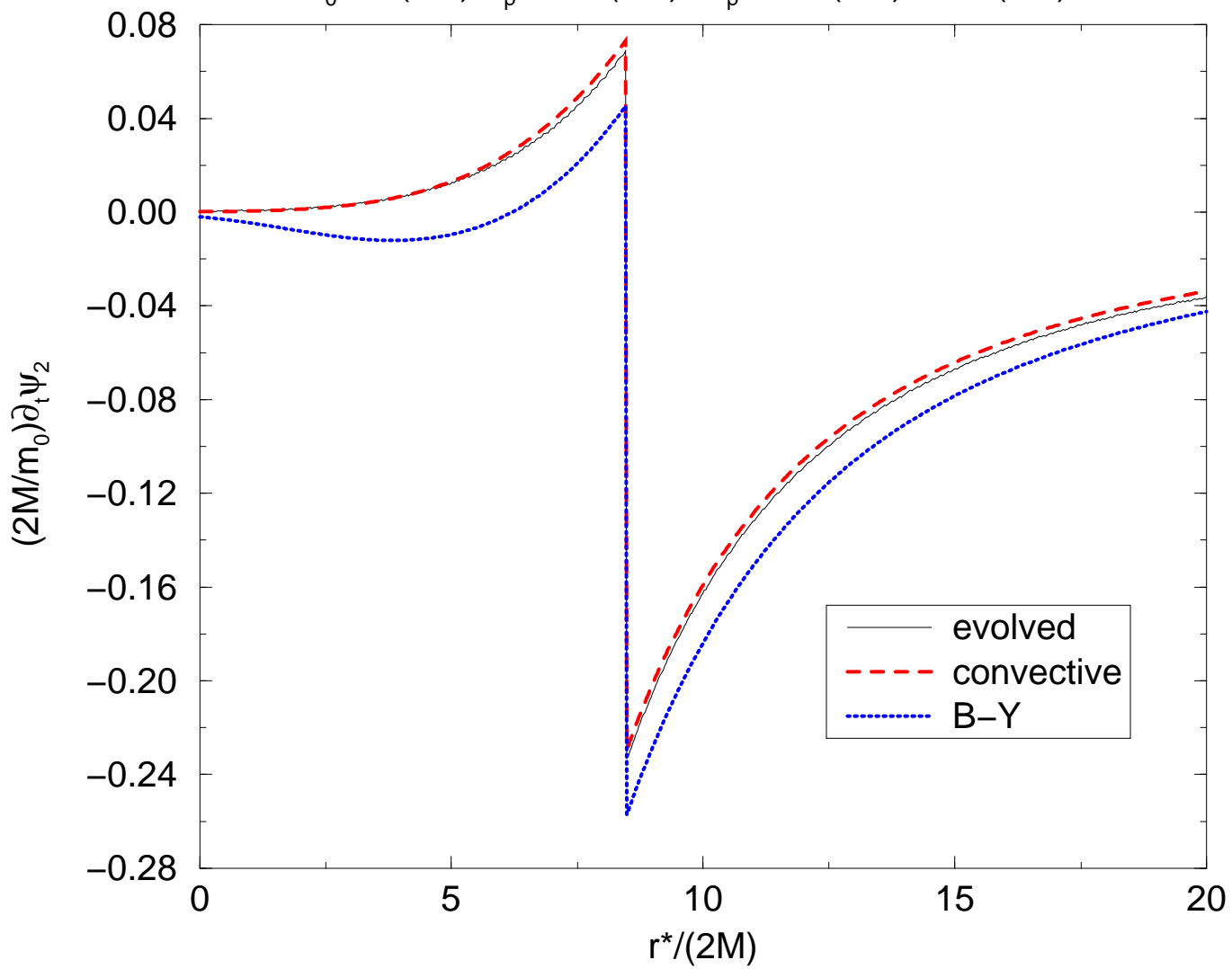
$r_0=1.5(2M)$, $r_p=1.22(2M)$, $r_p^*=-0.31(2M)$, $t=3.2(2M)$



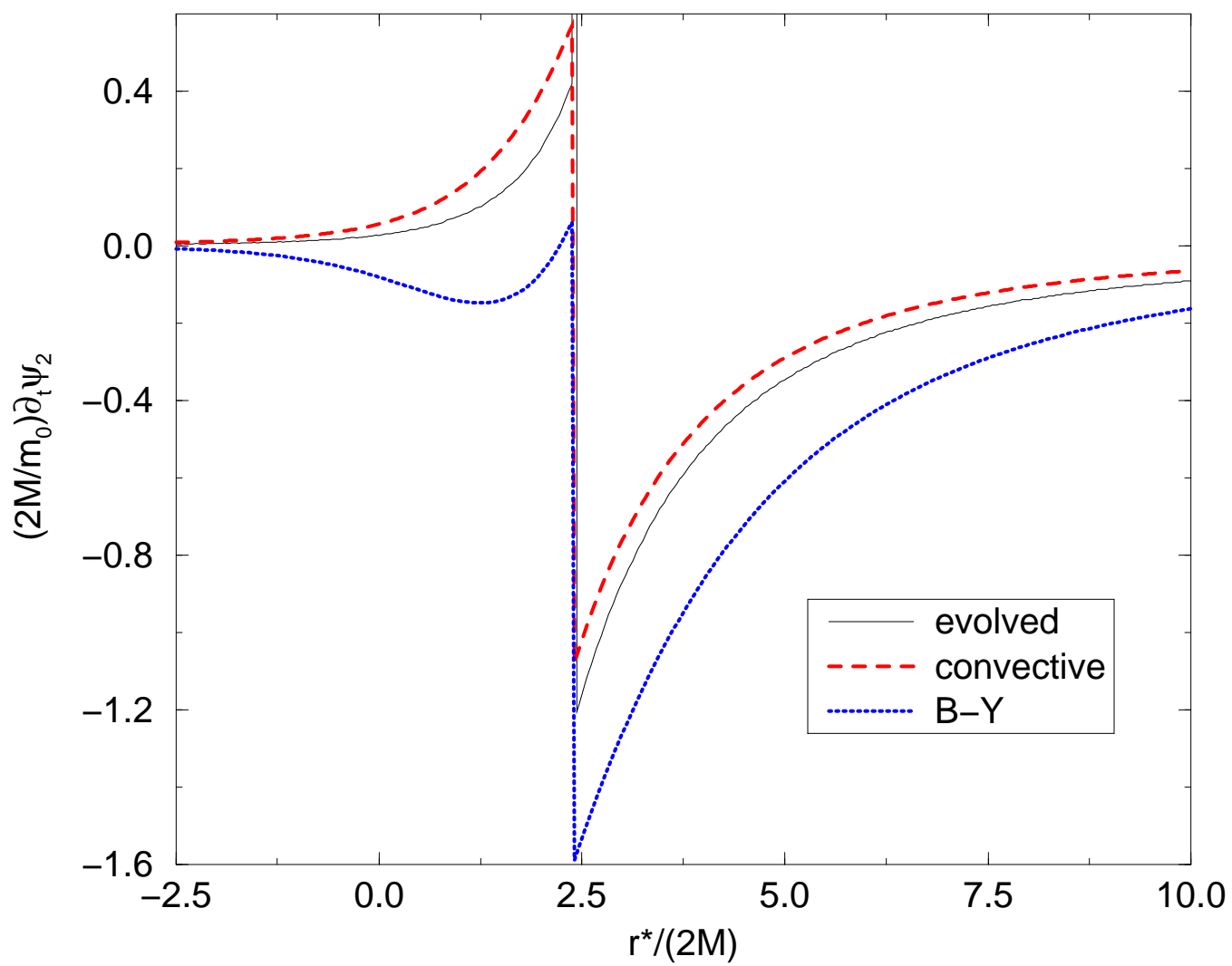
$r_0=1.5(2M)$, $r_p=1.09(2M)$, $r_p^*=-1.26(2M)$, $t=4.5(2M)$



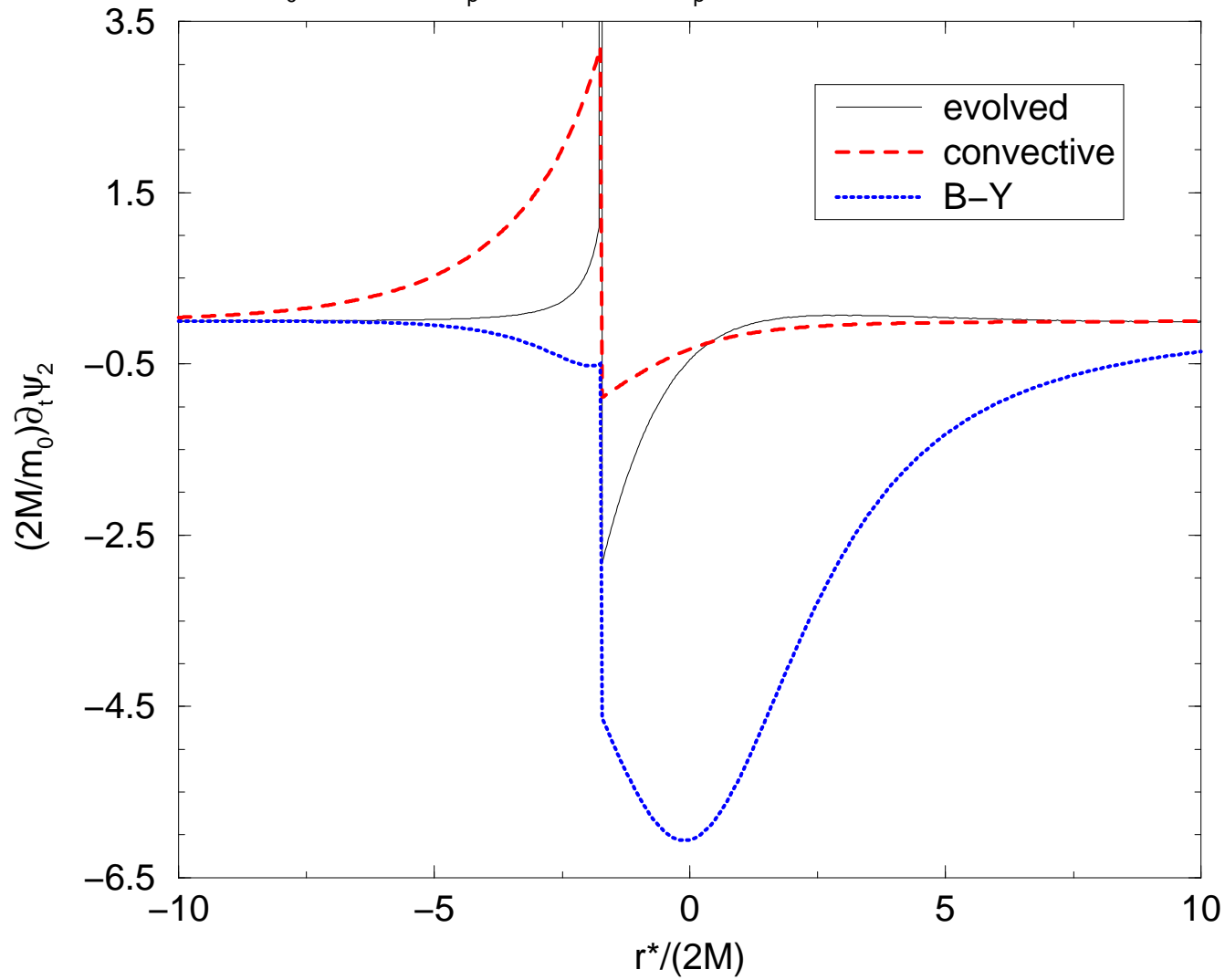
$r_0=15(2M)$, $r_p=6.73(2M)$, $r_p^*=8.47(2M)$, $t=82(2M)$



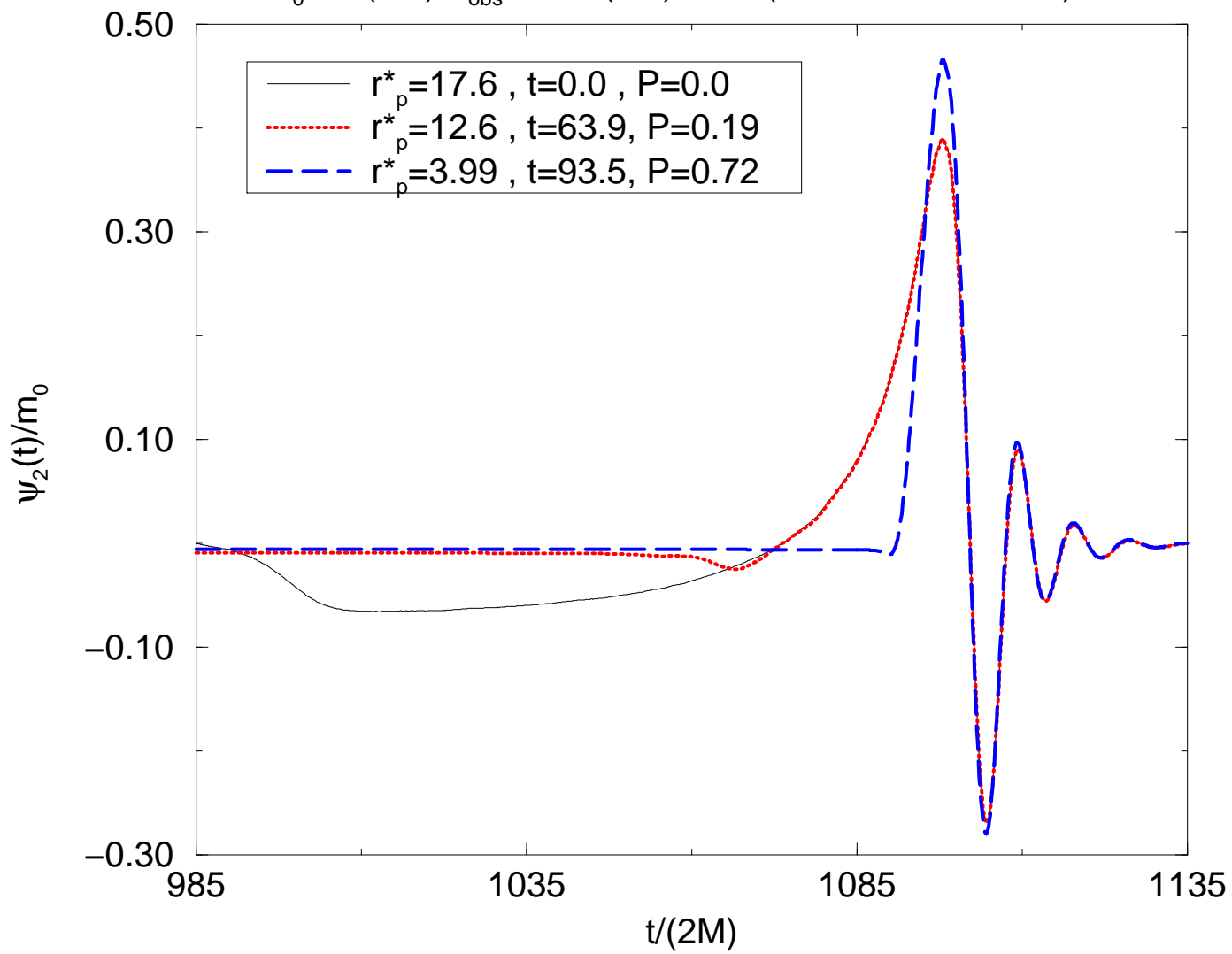
$r_0=15(2M)$, $r_p=2.21(2M)$, $r_p^*=2.40(2M)$, $t=96(2M)$



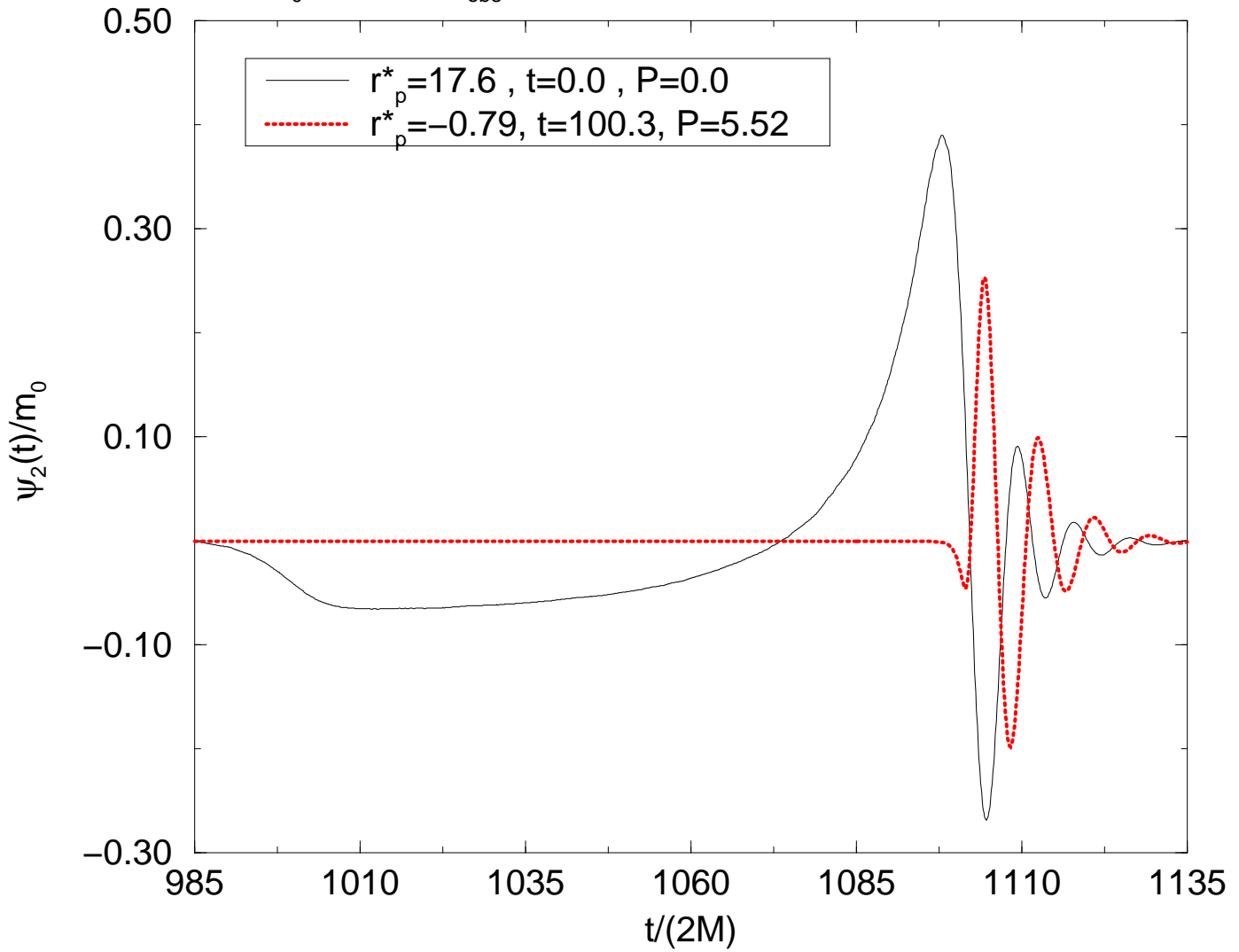
$r_0=15(2M)$, $r_p=1.06(2M)$, $r_p^*=-1.75(2M)$, $t=101(2M)$



$r_0=15(2M)$, $r_{\text{obs}}=1000(2M)$, $l=2$, (frozen-convective)



$r_0=15(2M)$, $r_{\text{obs}}=1000(2M)$, $l=2$, (frozen-convective)



$r_0=15(2M), l=2$

